Eur. Phys. J. Appl. Phys. **54**, 33510 (2011)
DOI: 10.1051/epjap/2011100469

THE EUROPEAN PHYSICAL JOURNAL APPLIED PHYSICS

Regular Article

Capturing EELS in the reciprocal space

C. Hébert[1,2,a], A. Alkauskas[1,2], S. Löffler[3], B. Jouffrey[4], and P. Schattschneider[4,5]

[1] Institute of Condensed Matter Physics, École Polytechnique Fédérale de Lausanne, Switzerland
[2] Interdisciplinary Center for Electron Microscopy, École Polytechnique Fédérale de Lausanne, Switzerland
[3] Institute of Solid State Physics, Vienna University of Technology, Austria
[4] LMSS-Mat, CNRS-UMR 8579, École Centrale Paris, Châtenay-Malabry, France
[5] University Service Centre for Transmission Electron Microscopy, Vienna University of Technology, Austria

Received: 22 November 2010 / Received in final form: 16 February 2011 / Accepted: 15 April 2011
Published online: 20 June 2011 –

Abstract. In this work two aspects of momentum-dependent electron energy loss spectrometry are studied, both in the core-loss and in the low-loss region. In the case of core losses, we focus on the demonstration and the interpretation of an unexpected non-Lorentzian behavior in the angular part of the double-differential scattering cross-section. The silicon L_3 edge is taken as an example. Using calculations we show that the non-Lorentzian behavior is due to a change in the wavefunction overlap between the initial and the final states. In the case of low losses, we first analyze the momentum-dependent loss functions of coinage metals Cu, Ag, and Au. We then demonstrate how advanced electronic structure calculations can be used to build simple models for the dielectric function that can then serve as a basis for the calculation of more complicated sample geometries.

1 Introduction

Electron energy loss spectrometry (EELS) in the transmission electron microscope (TEM) is a powerful technique, not only for the chemical quantification but also for the investigation of the electronic structure of materials [1]. Like photon absorption spectroscopies (optical, UV, or X-ray), EELS can probe electronic transitions from both valence and core electronic states. However, EELS has an additional degree of freedom: while the momentum transfer in the photon absorption is given by the momentum (and thus the energy) of that photon, the momentum transfer in EELS is independent of the energy loss. The momentum transfer is directly linked to the scattering angle and is therefore accessible in the diffraction plane of an electron microscope. Since these momenta can cover several Brillouin zones, this allows the observation of indirect electronic transitions. In Figure 1 a sketch of the scattering geometry in the TEM is shown.

"Capturing EELS in the reciprocal space" (i.e., measuring the momentum-dependent electronic response) not only brings a variety of new information but is also linked to new challenges, especially in terms of the interpretation. Experimental methods have been developed for the acquisition of angular-resolved EELS spectra like the HARECES by Zaluzec et al. [2]. Angular-resolved EELS has already been used, e.g., for the investigation of anisotropic materials [3–8]. Sometimes, anisotropy effects have to be avoided, e.g., when the goal is the determination of the sp^2/sp^3 ratio in different modifications of carbon [9]. Moreover, in reciprocal space one can select particular channeling conditions, giving rise to site-selective material characterization by choosing, for example, channeling or anti-channeling conditions [10].

In EELS, the key quantity which characterizes the inelastic scattering is the double-differential scattering cross-section (DDSC) $\partial^2\sigma/(\partial E\,\partial\Omega)(E,\mathbf{Q})$. The DDSC describes the probability of experiencing a certain energy loss E in a certain direction (unequivocally given by $\mathbf{Q}$) in the energy interval ∂E and the solid angle $\partial\Omega$. In both regions of the spectrum, i.e., for low-energy losses (low-loss, for short) and high-energy losses (core-loss, for short), the electron-electron interactions dominate inelastic scattering. In the low-loss region, where the collective behavior of the electron gas is often most important, the scattering is best described in terms of the macroscopic dielectric function $\varepsilon(\mathbf{Q},E)$. At variance, in the core-loss region the initial state is rather well defined and thus the localized description is often more appropriate. In this paper we discuss the momentum dependence of EEL spectra both in the core-loss and the low-loss region. In particular, we focus on challenges related to the interpretation of those spectra.

The paper is organized as follows. Section 2 deals with the momentum dependence of EELS in the core-loss region. It is shown that at larger scattering vectors, approaching the first Bragg spots, the commonly accepted Lorentzian behavior of the DDSC does not hold anymore.

[a] e-mail: cecile.hebert@epfl.ch

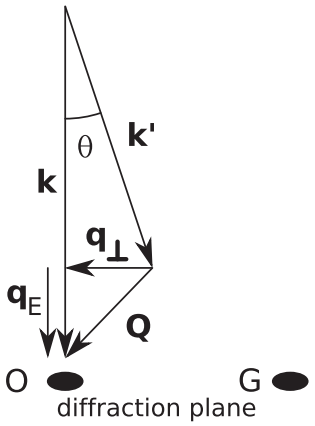

Fig. 1. Sketch of the scattering geometry in the TEM showing the incoming and the outgoing wave vectors, $\mathbf{k}$ and $\mathbf{k}'$, the wave vector transfer $\mathbf{Q}$ and two diffraction spots. $\mathbf{Q}$ is decomposed into its two components $\mathbf{q}_E$ and $\mathbf{q}_\perp$.

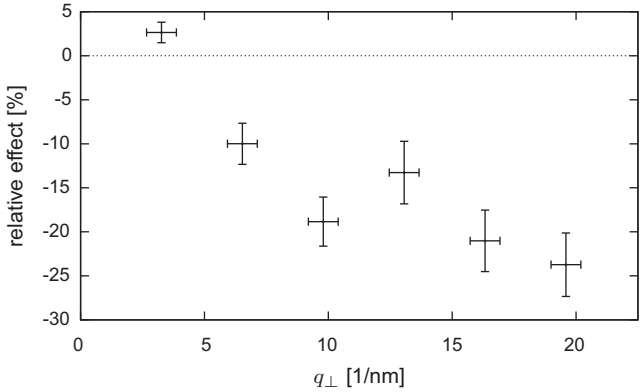

Fig. 2. Relative deviations from Lorentzian scattering behavior for the example of the Si L_3 edge. The specimen was 35 nm thick and oriented in a systematic row condition including the (2 2 0) diffraction spot. $q_\perp$ was chosen perpendicular to the systematic row. The error bars were derived from the quality of fit and the aperture used.

In Section 3, we will consider the low-energy part of the spectrum and review theoretical methods that can be used to calculate momentum-dependent loss functions of bulk systems. These are then applied to the metals Cu, Ag, and Au. In the second half of the section we show how these theoretical calculations provide insights that help constructing model dielectric functions, suitable for the analysis of low-dimensional systems. The paper ends with conclusions.

2 Angular dependence in core-loss EELS

As elaborated in, e.g., [11,12], the DDSC for inelastic electron scattering in single-electron, first-order Born approximation is given by

$$\frac{\partial^2\sigma}{\partial E\,\partial\Omega} = \frac{4\gamma^2}{a_0^2}\frac{k'}{k}\frac{S(\mathbf{Q},E)}{Q^4}, \tag{1}$$

where $\gamma = (1 - v^2/c^2)^{-1/2}$ is the relativistic factor, a_0 is the Bohr radius, k and k' are the incident and the outgoing wavenumbers, $\mathbf{Q}$ is the wave vector transfer, and S is the dynamic form factor (DFF) which is essentially derived from the transition matrix element of the sample electrons. For core losses, its full form is given in, e.g., [11,13].

Most noteworthy for off-axis experiments is the angular dependence of the DFF which is given by

$$[Y_\lambda^\mu(\mathbf{Q}/Q)\langle j_\lambda(Q)\rangle]^2,$$

where the Y_λ^μ are the spherical harmonics, λ is the transition order, and

$$\langle j_\lambda(Q)\rangle_{Elsj} = \int r^2 u_{ls}^E(r) j_\lambda(Qr) R_{js}(r)\mathrm{d}r \tag{2}$$

is the weighted wavefunction overlap integral, with the initial state wavefunction $R_{js}(r)$ and the final state wavefunction $u_{ls}^E(r)$. j_λ stands for the spherical Bessel functions.

Commonly, equation (2) is expanded into a Taylor series in Q and only the first-order term is retained. This leads to $\langle j_\lambda(Q)\rangle_{Elsj} \propto Q^\lambda$. In addition, one usually ignores non-dipolar transitions which have $\lambda \neq 1$. Taking the properties of the spherical harmonics into account, this then gives rise to the well-known Lorentzian angular dependence of the DDSC:

$$\frac{\partial^2\sigma}{\partial E\,\partial\Omega} = \frac{f(E)}{Q^2} = \frac{f(E)}{q_\perp^2 + q_E^2}, \tag{3}$$

which is the basis for many formulas for quantitative EELS analysis in the core-loss region [1,14,15]. Here, $Q^2 = q_\perp^2 + q_E^2$ with the characteristic momentum transfer $q_E = kE/(2\gamma T)$ used in the last equality. For comparison, $q_E \approx 0.72$ nm^{-1} for the Si $L_{2,3}$ edges is small – though not negligible – compared to values of $q_\perp$ used in the experiment and much smaller than the Bragg vector $|\mathbf{g}_{(2\,2\,0)}| \approx 32.7$ nm^{-1}.

However, a recent investigation has shown that for non-vanishing Q, which is always the case, since $Q \geq q_E$, this so-called dipole approximation does not strictly hold [16]. Figure 2 shows relative deviations from the Lorentzian on the energy scale. For this, spectra recorded at different $q_\perp$ were compared. By dividing spectra by each other, the angular independent prefactor $f(E)$ cancels out in the dipole approximation and one would be left with only the Lorentzian behavior. The relative deviations given in Figure 2 are determined from the difference between the quotient of spectra and a fitted Lorentzian curve.

It can be seen that the relative deviations are generally negative and can be up to about 30% even at relatively small scattering angles of the order of the Bragg angle. These deviations are also material-specific [16].

For very large angles, non-dipolar transitions with $\lambda \neq 1$ can play an important role [17], owing to the fact that their leading terms behave as $Q^{2\lambda-4}$. In the present case, this was ruled out by numerical calculations using the code `WIEN2k` [18], as the contributions from

https://doi.org/10.1051/epjap/2011100469 Published online by Cambridge University Press

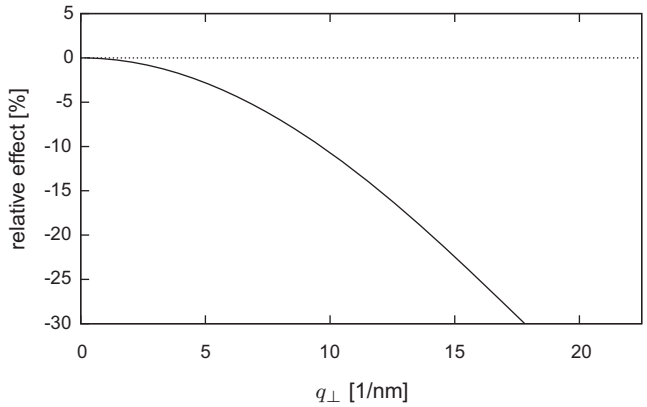

Fig. 3. Relative deviations from the Lorenzian behavior as calculated by using the full form of equation (2) and Slater-type orbitals for the example of the Si L_3 edge.

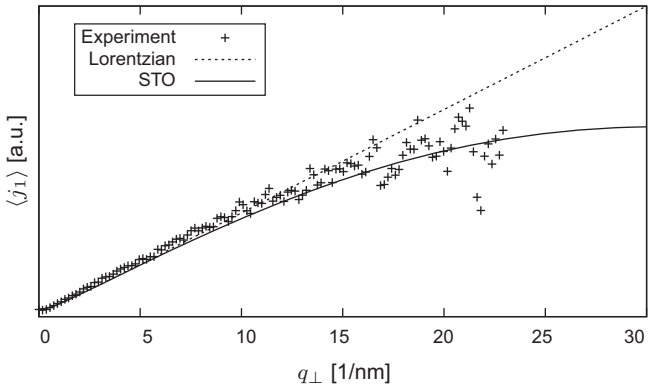

Fig. 4. Plot of $\langle j_1(Q) \rangle$ as derived from an energy-filtered selected area diffraction pattern of the Si L_3 edge. The straight line shows the Lorentzian behavior and the curved line shows the results of STO calculations.

those terms were smaller than 1% in the angular range investigated in the experiment. Consequently, only dipole-allowed transitions with $\lambda = 1$ were used for this work.

Experimental inelastic electron scattering is complicated by the strong elastic scattering effects, leading to channeling behavior of both the incident and the outgoing beam. Since this effect is well understood, it can easily be dealt with in numerical simulations [16,19]. Calculations show that for the relatively small thickness of the specimens used for this work, the influence is of the order of 2%. Thus, it is smaller than the typical error bars in this experiment (see Fig. 2).

The real cause for these observed deviations can be found in higher-order terms of the expansion of equation (2). For non-vanishing Q, it is possible to measure the influence of the wavefunction overlap of the initial and final states. Indeed, calculations using simple Slater-type orbitals (STO) [20] yield similar deviations as the ones observed experimentally. Figure 3 shows that they are negative and of the same order of magnitude.

Furthermore, it is possible to directly image $\langle j_\lambda(Q) \rangle$ by means of energy-filtered selected area diffraction (EFSAD). Using the three window method [1], one can directly obtain a map of the excitation edge in the reciprocal space, from which it is straightforward to extract a line profile. Figure 4 shows such a line profile. It is clearly visible that at momentum transfers of the order of $20\,\mathrm{nm}^{-1}$, the experimental curve deviates significantly from the Lorentzian line, but is in better agreement with the STO calculations.

Furthermore, it is possible to directly image $\langle j_1(Q) \rangle$ by means of energy-filtered selected area diffraction (EFSAD). Using the three window method [1], one can directly obtain a map of the excitation edge in the reciprocal space, from which it is straightforward to extract a line profile. Figure 4 shows such a line profile. It is clearly visible that at momentum transfers of the order of $20\,\mathrm{nm}^{-1}$, the experimental curve deviates significantly from the Lorentzian line, but is in better agreement with the STO calculations.

3 Angular dependence in low-loss EELS

In the low-loss regime the inelastic electron scattering is best described using the dielectric formulation. The DDSC for the momentum transfer $\mathbf{Q}$ and the energy loss E (the equivalent of Eq. (1)) is proportional to $|v(\mathbf{Q})|^2 S(\mathbf{Q}, E)$, where $S(\mathbf{Q}, E)$ is the dynamic structure factor of the material and $v(\mathbf{Q})$ is the Fourier transform of the Coulomb interaction ($\sim 1/Q^2$) [1,21]. The momentum transfer $\hbar\mathbf{Q}$ can in principle have any value, and $S(\mathbf{Q}, E) \sim Q^2$ for small $\mathbf{Q}$. However, apart from the "trivial" $1/Q^2$ dependence (similar to the previous section), there is an intrinsic momentum dependence of the DDSC in the low-loss case due to properties of the inhomogeneous electron gas, described by $S(\mathbf{Q}, E)$. For the periodic solid, the dynamic structure factor is proportional to the density response function χ via $S(\mathbf{Q}, E) = -2\hbar\,\mathrm{Im}\,\chi_{\mathbf{G},\mathbf{G}}(\mathbf{q}, E)$, where $\mathbf{Q} = \mathbf{G} + \mathbf{q}$, $\mathbf{G}$ is the reciprocal lattice vector so that $\mathbf{q}$ is confined to the first Brillouin zone. Thus, the DDSC can be expressed as:

$$\frac{\partial^2\sigma}{\partial E\,\partial\Omega} \sim -|v(\mathbf{Q})|^2\,\mathrm{Im}\,\chi_{\mathbf{G},\mathbf{G}}(\mathbf{q}, E) = v(\mathbf{Q})\mathrm{Im}\big(-\varepsilon^{-1}_{\mathbf{G},\mathbf{G}}(\mathbf{q}, E)\big), \quad (4)$$

where the inverse dielectric matrix is:

$$\varepsilon^{-1}_{\mathbf{G},\mathbf{G}'}(\mathbf{q}, E) = \delta_{\mathbf{G},\mathbf{G}'} + v(\mathbf{q}+\mathbf{G})\chi_{\mathbf{G},\mathbf{G}'}(\mathbf{q}, E). \quad (5)$$

The term $L(\mathbf{Q}, E) = \mathrm{Im}\big(-\varepsilon^{-1}_{\mathbf{G},\mathbf{G}}(\mathbf{q}, E)\big)$ is called the loss function. While the DDSC has an additional prefactor $1/Q^2$, the loss function is a convenient quantity since it is dimensionless, and furthermore, loss functions for any $\mathbf{Q}$ obey the so-called *f*-sum rule with a Q-independent integration constant. At variance, dynamic structure factors are more convenient in inelastic X-ray spectroscopy since they are directly proportional to the double-differential scattering cross-section.

As seen from equation (4), the crucial ingredient to determine the double-differential scattering cross-section in the low-loss regime is the calculation of χ. In this work,

https://doi.org/10.1051/epjap/2011100469 Published online by Cambridge University Press

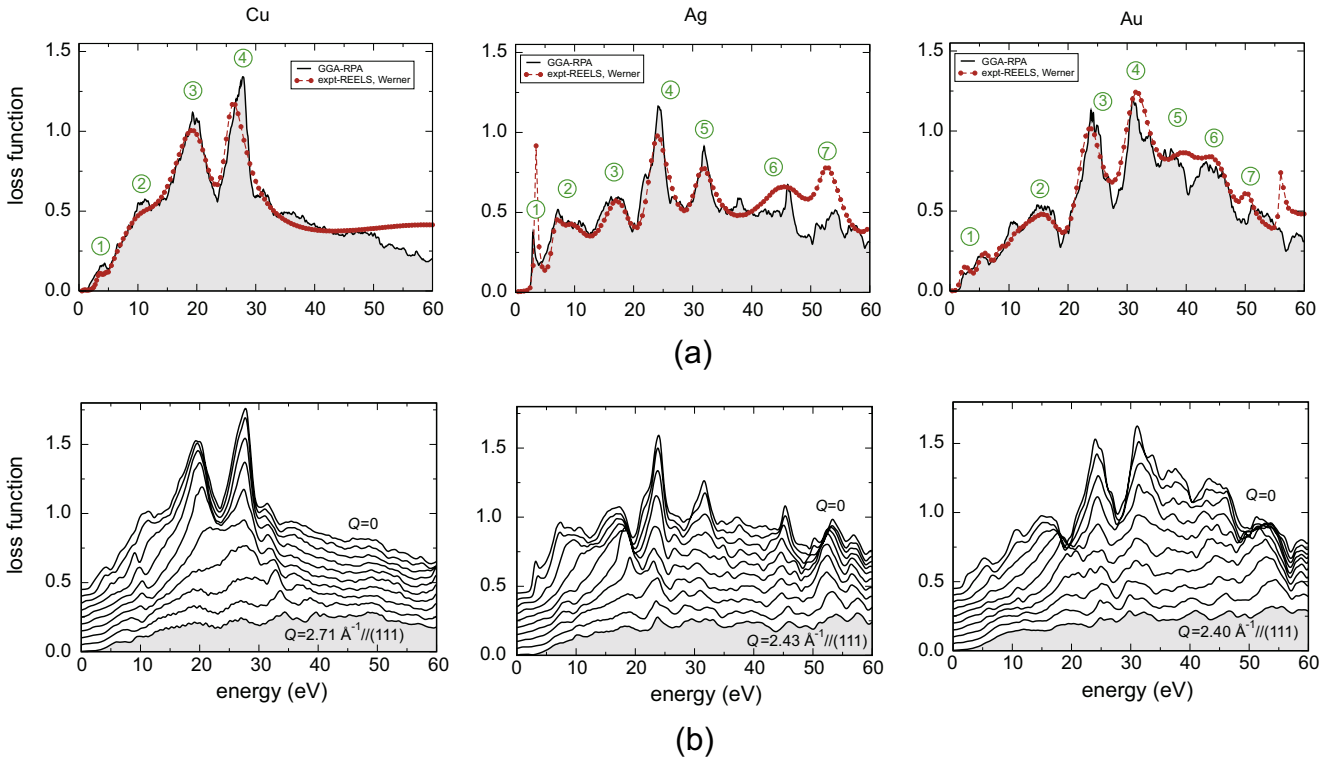

Fig. 5. (Color online) (a) Calculated loss functions of bulk Cu, Ag, and Au for small momentum transfers (solid lines), compared with experimental reflections EELS data of references [28,29]; (b) calculated momentum-dependent loss functions of bulk Cu, Ag, and Au. Adapted from reference [24].

we have used the random phase approximation (RPA), in which, symbolically, the interacting density response function is given by $\chi = \chi_0/(1 - v\chi_0)$ [22,23]. Here χ_0 is the response function of the non-interacting Kohn-Sham system. The inclusion of exchange-correlation effects into the dynamic response via the adiabatic local density approximation kernel changes the result very little. These will be discussed elsewhere [24]. In the present section, our calculations have been performed with the full-potential linearized augmented plane-wave code Exciting [25,26]. Local-field effects were included. The non-interacting density response functions have been calculated using the single-electron wavefunctions and eigenvalues obtained from density functional theory calculations. For the latter, the generalized-gradient approximation (GGA) of reference [27] has been used for the exchange-correlation potential. More details on the methodology can be found in, for example, references [22,23].

In Figure 5a, we present the calculated loss functions for Cu, Ag, and Au for small momentum transfers, compared with experimental data obtained from reflection electron energy loss spectroscopy (REELS) by Werner et al. [28,29]. All three metals exhibit a complex multi-peak structure in the loss function. In the energy range 0–60 eV, 4 well-pronounced peaks are distinct in the case of Cu, 7 in the case of Ag, and 7–8 in the case of Au. Peak (1) of Ag, and, to a lesser extent, peak (1) of Au, peak (2) of Ag, and peak (1) of Cu, originate from the vanishing (or small) real part of the dielectric function and can thus be classified as plasmon peaks [30]. However, except in Ag, these excitations are severely damped. At variance, other well-pronounced peaks are due to inter-band transitions from occupied d states to the unoccupied continuum with large density of states [30,31]. Overall, the agreement between the calculated and measured loss functions is very good. One of the most important disagreements is the intensity and also the position of the peak (1) of Ag, which we discuss in some detail below. Noticeable other discrepancies occur for peaks (6) and (7) of Ag. For the latter two, theoretical values of peak positions are very good, but peak intensities are substantially under-estimated. Similar disagreement is evident in the case of Au for peaks (7) and (8). While it is not impossible that theory does not capture several important effects at higher energies, the discrepancy can also stem from a small inaccuracy of experimental loss functions. Indeed, in order to obtain the bulk loss function from REELS, complicated mathematical algorithms have to be used to extract the bulk contributions to the loss function and, in addition, also to estimate its component for small momentum transfers [28,29].

Given this overall good agreement between calculated and measured loss functions of all three metals at small momentum transfers, in Figure 5b, we show momentum-dependent loss functions. For all three metals the overall picture is very similar. As the momentum transfer increases, the peaks in the loss function decrease in intensity. Thus, the loss functions become increasingly

https://doi.org/10.1051/epjap/2011100469 Published online by Cambridge University Press

featureless for higher momentum transfers. At variance, the tails of loss functions persist to increasingly higher energies, so that the loss functions extend to larger energies. This guarantees that the f-sum rule is always satisfied. Such behavior is universal for all metals and these basic trends are already evident from the Lindhard dielectric function of the homogenous electron gas [32]. Experimental measurements of momentum-dependent loss functions of Cu, Ag, and Au are in progress [33].

The reasons of an inaccurate description of the plasmon peak (1) in the case of Ag are understood [34,35]. The main problem stems from the calculation of χ_0. Indeed, the band structure of Ag calculated with the GGA exchange-correlation potential is not accurate enough. Most importantly, due to the self-interaction error of GGA, Ag $4d$ states are (i) under-bound by about 1 eV and (ii) also somewhat broader than can be deduced from photo-emission measurements or more accurate calculations. This problem can be solved, for instance, by correcting the single-particle eigenvalues using the many-body perturbation theory in the GW approximation [35]. This gives significant improvement in the position and the intensity of the plasmon peak [35]. In addition, the calculated plasmon dispersion is in excellent agreement with available experimental data [24,36,37].

In this work, to illustrate general features related to response functions in metals, we study the plasmon dispersion in Ag by first devising the model dielectric function for energies <5 eV. More accurate calculations [24] show that local-field effects are negligible in this energy range, and thus instead of dealing with the inverse dielectric matrix, we can directly deal with scalar dielectric functions. The model dielectric function of Ag is defined as:

$$\varepsilon^{\text{Ag,model}}(\mathbf{Q}, E) = \varepsilon^{\text{Lindhard}}(\mathbf{Q}, E) + \varepsilon^{\text{inter-band}}(E). \quad (6)$$

Here, $\varepsilon^{\text{Lindhard}}(\mathbf{Q}, E)$ is the Lindhard dielectric function, which describes the intra-band contribution (the only free parameter is the effective electron mass in the sp band, here set to $m = 0.95m_e$, the "optical electron mass" in Ag), while $\varepsilon^{\text{inter-band}}$ is the inter-band contribution. The latter is taken to be momentum-independent and is calculated using the methodology outlined above, in which in addition the single-electron eigenvalues were approximately corrected using the GW calculations of reference [35].

In Figure 6, we show the two-dimensional plot of the plasmon dispersion, calculated using the model dielectric function. The plasmon dispersion can be fitted using the quadratic equation $\omega(Q) = \Omega_p + \alpha\hbar Q^2/m$, and the fitting procedure yields values of $\Omega_p = 3.45$ eV, $\alpha = 0.50$. These values are in very good agreement with those obtained from full calculations [24], and present a significant improvement over the results obtained using the GGA band structure. Comparisons with more accurate calculations [24] show that the model dielectric function (Eq. (6)) is accurate up to momentum transfers of $Q = 0.20$–0.25 Å^{-1}. At higher momentum transfers (0.25–0.40 Å^{-1}) the plasmon dispersion becomes significantly non-quadratic.

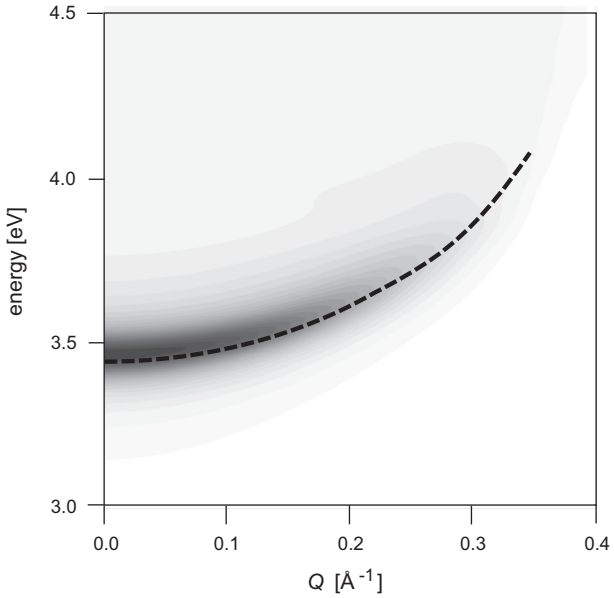

Fig. 6. Plasmon dispersion in bulk Ag, calculated using the model dielectric function, equation (6).

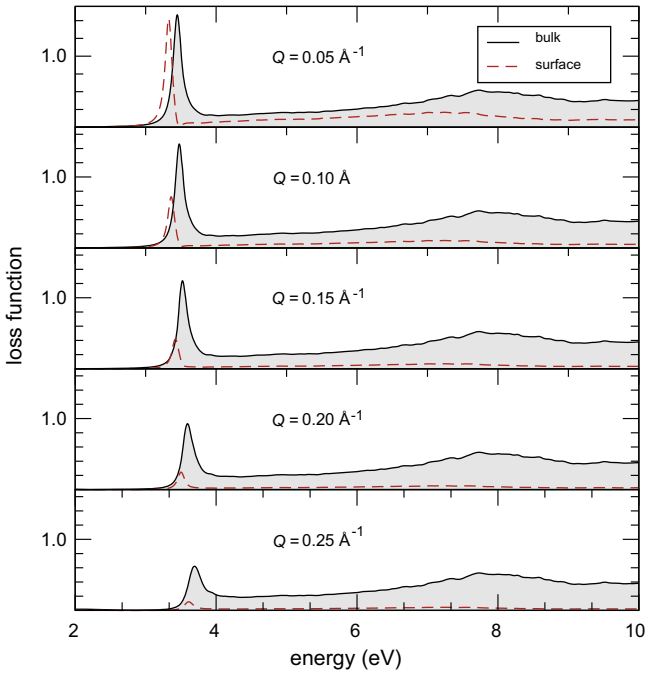

Fig. 7. (Color online) Bulk and surface contributions to loss functions of the silver slab of thickness $d = 100$ Å for varying momentum transfers.

This behavior comes from the momentum dependence of the inter-band term in equation (6).

The dielectric function in equation (6) can also be used to model loss functions of nanostructures. In Figure 7, we show the loss function of a silver slab of thickness $d = 100$ Å compared to the bulk loss function for varying momentum transfers. The bulk loss function is defined as

https://doi.org/10.1051/epjap/2011100469 Published online by Cambridge University Press

$L_{\rm bulk} = -{\rm Im}(\varepsilon^{-1})$, whereas we define the "effective" loss function of the slab as:

$$L_{\rm slab} = \frac{2}{Qd}{\rm Im}\left[-\frac{(1-\varepsilon)^2}{\varepsilon(1+\varepsilon)}\right]. \quad (7)$$

The meaning of this quantity is that the term $\sim L_{\rm slab}/Q^2$ gives the surface contribution to the double-differential cross-section [38] (which is multiplied by 2 to account for two surfaces in the slab), in exactly the same manner, as the term $\sim L_{\rm bulk}/Q^2$ gives the bulk contribution. As seen in Figure 7 this formulation yields automatically the frequency of the surface plasmon, which is found to be 0.12 eV below the bulk plasmon, in excellent agreement with experimental data [39]. The surface contribution decreases faster than the bulk contribution due to the prefactor $1/Qd$, which is a well-established experimental fact. Such simple models can serve as a good starting point for more accurate calculations, for example those recently reviewed in reference [40]. This approach is particularly promising for modelling the optical properties of metallic nanoparticles of various shapes and sizes [41,42].

4 Conclusion

In this paper we have considered two unconventional aspects of the angular-resolved EELS. In the core-loss region, noticeable deviation from the universally accepted Lorentzian behavior of the angular distribution of the double-differential cross-section has been demonstrated for the Si L_3 edge. This unexpected finding can be explained by estimating the overlap between the initial and the final states using Slater-type orbitals appropriate to Si. It is therefore expected that the deviation from the Lorentzian has a strong dependence on the material and the edge studied. Further investigations via the band structure theory are envisaged as they would also take into account the changes due to the electronic structure of the solid. For the low-loss region, we have first analyzed the momentum-dependent loss functions of coinage metals. We have showed that the complex structure of loss functions mainly originates from inter-band transitions. We have also showed how accurate electronic structure calculations could be used to build simpler models that can be, in turn, fed into more generalized calculation schemes capable of dealing with complicated sample geometries. This is a very promising approach for the investigation of nanostructures like silver or gold nanoparticles.

This work was supported by the Swiss NSF (Grant No. 20021-120308) and the Austrian Science Fund (FWF) (Grant No. I543-N20).

References

1. R.F. Egerton, *Electron Energy-Loss Spectroscopy in the Electron Microscope*, 2nd edn. (Plenum Press, New York, 1996)
2. N.J. Zaluzec, Y. Ito, R.E. Cook, D.J. Miller, Microsc. Microanal. **12**, 978 (2006)
3. S. Waidmann, M. Knupfer, B. Arnold, J. Fink, A. Fleszar, W. Hanke, Phys. Rev. B **61**, 10149 (2000)
4. G. Radtke, Ultramicroscopy **108**, 893 (2008)
5. G. Radtke, G.A. Botton, J. Verbeeck, Ultramicroscopy **106**, 1082 (2006)
6. C. Witte, N.J. Zaluzec, L.J. Allen, Ultramicroscopy **110**, 1390 (2010)
7. R.F. Klie, L.D. Cooley, Y. Zhu, Microsc. Microanal. **10**, 838 (2004)
8. D.S. Su, C. Hébert, M. Willinger, R. Schlögl, Micron **34**, 227 (2003)
9. J. Zhang, D. Su, A. Zhang, D. Wang, R. Schlögl, C. Hébert, Angew. Chem. Int. Ed. **46**, 7319 (2007)
10. O.L. Krivanek, M.M. Disko, J. Taftø, J.C.H. Spence, Ultramicroscopy **9**, 249 (1982)
11. P. Schattschneider, S. Rubino, C. Hébert, J. Rusz, J. Kuneš, P. Novák, E. Carlino, M. Fibrizioli, G. Panaccione, G. Rossi, Nature (London) **441**, 486 (2006)
12. P. Schattschneider, M. Nelhiebel, H. Souchay, B. Jouffrey, Micron **31**, 333 (2000)
13. D.K. Saldin, P. Rez, Philos. Mag. B **55**, 481489 (1987)
14. R. Knippelmeyer, P. Wahlbring, H. Kohl, Ultramicroscopy **68**, 25 (1997)
15. M. Stöger-Pollach, Micron **39**, 1092 (2008)
16. S. Löffler, I. Ennen, F. Tian, P. Schattschneider, N. Jaouen, Ultramicroscopy (2011) (in press), DOI: 10.1016/j.ultramic.2011.03.006
17. J.M. Auerhammer, P. Rez, Phys. Rev. B **40**, 2024 (1989)
18. P. Blaha, K. Schwarz, G. Madsen, D. Kvasnicka, J. Luitz, *Wien2k, an augmented plane wave + local orbitals program for calculating crystal properties* (Techn. Universität Wien, Austria, 2001), http://www.wien2k.at
19. S. Löffler, P. Schattschneider, Ultramicroscopy **110**, 831 (2010)
20. J.C. Slater, Phys. Rev. **36**, 57 (1930)
21. D. Pines, *Elementary Excitations in Solids* (W.A. Benjamin, Inc., New York, 1964)
22. A.A. Quang, A.G. Eguiluz, Phys. Rev. Lett. **70**, 3955 (1993)
23. G. Onida, L. Reining, A. Rubio, Rev. Mod. Phys. **74**, 601 (2002)
24. A. Alkauskas, S.D. Schneider, S. Sagmeister, C. Ambrosch-Draxl, C. Hébert, in preparation
25. S. Sagmeister, C. Ambrosch-Draxl, Phys. Chem. Chem. Phys. **11**, 4451 (2009)
26. C. Ambrosch-Draxl et al., http://exciting-code.org
27. J.P. Perdew, K. Burke, M. Ernzerhof, Phys. Rev. Lett. **77**, 3865 (1996)
28. W.S.M. Werner, M.R. Went, M. Vos, K. Glantschnig, C. Ambrosch-Draxl, Phys. Rev. B **77**, 161404 (2008)
29. W.S.M. Werner, K. Glantschnig, C. Ambrosch-Draxl, J. Phys. Chem. Ref. Data **38**, 1013 (2009)
30. A. Alkauskas, S.D. Schneider, S. Sagmeister, C. Ambrosch-Draxl, C. Hébert, Ultramicroscopy **110**, 1081 (2010)
31. I. Campillo, A. Rubio, J.M. Pitarke, Phys. Rev. B **59**, 12188 (1999)
32. W. Schülke, H. Nagasawa, S. Mourikis, P. Lanzki, Phys. Rev. B **33**, 6744 (1986)
33. S.D. Schneider et al., in preparation

34. M.A. Cazalilla, J.S. Dolado, A. Rubio, P.M. Echenique, Phys. Rev. B **61**, 8033 (2000)
35. A. Marini, R. Del Sole, G. Onida, Phys. Rev. B **66**, 115101 (2002)
36. A. Otto, E. Petri, Solid State Commun. **20**, 23 (1976)
37. P. Zacharias, K.L. Kliewer, Solid State Commun. **18**, 23 (1976)
38. R.H. Ritchie, Phys. Rev. **106**, 874 (1957)
39. A. Liebsch, Phys. Rev. Lett. **71**, 145 (1993)
40. F.J. García de Abajo, Rev. Mod. Phys. **82**, 209 (2010)
41. J. Nelayah, M. Kociak, O. Stephan, F.J. García de Abajo, M. Tence, L. Henrard, D. Taverna, I. Pastoriza-Santos, L.M. Liz-Marzan, C. Colliex, Nat. Phys. **3**, 348 (2007)
42. B. Schaffer, K. Riegler, G. Kothleitner, W. Grogger, F. Hofer, Micron **40**, 269 (2009)

https://doi.org/10.1051/epjap/2011100469 Published online by Cambridge University Press